J. Fluid Mech. (2011), *vol.* 673, *pp.* 121–131. © Cambridge University Press 2011
doi:10.1017/S0022112011000048

Ripple and dune formation in rivers

M. COLOMBINI† AND A. STOCCHINO

Dipartimento di Ingegneria delle Costruzioni, dell'Ambiente e del Territorio,
Università degli Studi di Genova Via Montallegro 1, 16145 Genova, Italy

(Received 20 October 2010; revised 25 November 2010; accepted 23 December 2010;
first published online 2 March 2011)

A linear stability analysis for dune and ripple formation is presented that implements a rotational two-dimensional flow model valid in the smooth as well as in the transitional and rough flow regimes. Sediment is assumed to be transported as bedload, disregarding the role of suspension. Therefore, the main mechanism driving instability, for both ripples and dunes, is the phase lag between bed shear stress and bed elevation. Ripples are shown to be confined to relatively low values of the Shields parameter and of the particle Reynolds number. For higher values of the Shields parameter and of the particle Reynolds number (and thus of the Froude number and of the roughness Reynolds number), ripples are replaced by dunes. The present analysis ultimately allows for a successful unification of the theories of dune and ripple formation and for a clarification of the debated role of ripples on the formation of dunes. A good agreement between predicted and observed wavelengths for both ripples and dunes is found.

Key words: instability, river dynamics, sediment transport

1. Introduction

A variety of sediment waves develops from an initially flat bed when a uniform flow over an erodible bed is considered. They can be classified in terms of the characteristics of the bedforms (e.g. wavelength, shape, upstream or downstream propagation) and in terms of the characteristics of the flow (e.g. subcritical or supercritical, hydraulically smooth or rough regime, free-surface waves associated with the bed waves) or of the sediment transport (e.g. bed versus suspended load). In general, more than one aspect is needed to mark the distinction.

Among transverse bedforms, for instance, we can distinguish between dunes and anti-dunes, which possess similar wavelengths, by means of the flow regime (subcritical and supercritical, respectively) and of the amplitude and phase of free-surface undulations with respect to bed undulations (smaller and out of phase for dunes, larger and in phase for anti-dunes).

If we now consider dunes and ripples, they both appear in the subcritical regime and propagate downstream, but it is possible to discriminate ones from the others in terms of their characteristic wavelengths, ripples typically being about one order of magnitude shorter than dunes. It may be useful to report here the definition of dunes given by Guy, Simons & Richardson (1966) in their remarkable experimental work: 'Dunes are bed features larger than ripples that are out of phase with any water-surface gravity waves that accompany them. Dunes generally form at larger

† Email address for correspondence: col@dicat.unige.it

https://doi.org/10.1017/S0022112011000048 Published online by Cambridge University Press

flow and sediment transport rates than do ripples; however, ripples often form on the upstream slopes of dunes at smaller rates of flow'. About half a century later, this distinction, albeit being evident to the experimenters, is still debated. Indeed, as Raudkivi (2007) writes: 'the change from ripples to dunes is terra incognita'. Nonetheless, when attempting to distinguish dunes from ripples, the only strong argument available is that of the different wavelengths, which persists also when both bedforms appear together.

From the theoretical point of view, we restrict our attention to linear stability analyses, which have proved to be a formidable tool to predict the existence regions of bedforms in the space of the relevant physical parameters and their characteristic wavelengths. However, no information can be gathered on bedform amplitudes at a linear level.

The first attempt to describe ripple formation by means of a linear stability analysis, dates back to Richards (1980), who developed a rotational flow model under hydraulically rough conditions, showing that, at the same value of the Froude number, two separate modes of instability exist. The first mode, characterized by wavelengths scaling with the flow depth, was easily associated with dunes, while the second mode, with typical wavelengths scaling with the bed roughness, was postulated to correspond to ripples. Following Engelund & Fredsøe (1982), who suggested that ripples should be associated with the hydraulically smooth flow regime, Sumer & Bakioglu (1984) carried out a linear theory specifically formulated to investigate ripple formation. In particular, the flow model was developed to handle smooth as well as transitional flow regimes, whereas the role of the flow depth was disregarded. One of the major outcomes of their analysis was that the ripple wavelength should scale with the thickness of the viscous sublayer rather than with the bed roughness. However, both the above analyses predicted a wavelength of maximum amplification for ripples that were one or two orders of magnitude shorter than those observed in the laboratory. It is worth noting that Richard's analysis was restricted to the hydraulically rough regime, while Sumer & Bakioglu's theory was developed in the limit of vanishing Froude number (infinite flow depth).

It has been recently questioned (Fourrière, Claudin & Andreotti 2010) whether dunes and ripples are the result of an independent process of instability or ripples have to be considered as simple precursors of dunes, the latter being only produced by a mechanism of nonlinear pattern coarsening. Indeed, small amplitude sediment waves have been observed to lengthen as they grow (Coleman & Melville 1996). In the present work, the theory of Colombini (2004) is extended to cover the case of smooth and transitional flow regimes, aiming at the description of the process of both ripple and dune formation in the same framework of instability. In this regard, the work of Kobayashi & Madsen (1985) is also worth mentioning, who first attempted to follow this line of thought without succeeding to improve the prediction of ripple wavelength, probably due to the lack of a suitable sediment transport model.

2. Experimental observations on ripples and dunes

The most comprehensive collection of flume experiments concerning finite-amplitude bedforms is the Fort Collins data set of Guy *et al.* (1966), which covers a relatively wide range of grain sizes, flow depths and Froude numbers.

As already discussed by Colombini & Stocchino (2008), the comparison of the results of the stability analysis with experimental observations requires evaluation of the shear stress acting on a plane bed, thus eliminating the contributions due to the

https://doi.org/10.1017/S0022112011000048 Published online by Cambridge University Press

form resistance and sidewalls. Hence, an equivalent uniform flow has been sought relating the friction coefficient of the bed region f_b, or equivalently the conductance coefficient C, to the corresponding hydraulic radius r_b^* through the following equation valid for the transitional regime:

$$C = \frac{U^*}{u_b^*} = \sqrt{\frac{8}{f_b}} = \frac{1}{\kappa} \ln \left[\left(\frac{a_r r_b^*}{k_s^*} \right)^{1-\beta} \left(\frac{Re\sqrt{f_b}}{a_s} \right)^{\beta} \right], \quad Re = \frac{4U^* r_b^*}{\nu}, \tag{2.1}$$

where U^* is the area velocity, u_b^* is the bed friction velocity, Re is the Reynolds number of the flow, ν is the kinematic viscosity of the fluid and κ is the Von Kármán constant, taken as 0.4. Note that, here and in the following, variables with a star superscript are to be intended as dimensional. The constants a_s and a_r, which are representative of the behaviour in the smooth and rough regime in infinitely wide channels, are set equal to 3.41 and 11.09, respectively (ASCE Task Committee 1963). Finally, the weighting factor β varies from 0 to 1 as the flow regime changes from hydraulically rough to hydraulically smooth. Following Cheng (2008) we set

$$\beta = \exp\left[-0.11(\ln Re_k)^{\frac{5}{2}}\right], \quad Re_k = \frac{u_b^* k_s^*}{\nu} = \sqrt{\frac{f_b}{8}} Re \frac{k_s^*}{4r_b^*}, \tag{2.2}$$

where k_s^* is the roughness height and Re_k is the roughness Reynolds number.

The above procedure allows for the implicit determination of the hydraulic radius of the bed region r_b^* and, in turn, of all the quantities appearing in (2.1)–(2.2). Note that, as far as the bed shear stress is concerned, r_b^* takes the role of the characteristic vertical length scale of the flow. Among the parameters that are relevant for the sediment transport, we recall here the Shields parameter θ and the particle Reynolds number Re_p:

$$\theta = \frac{u_b^{*2}}{(s-1)gd^*}, \quad Re_p = \frac{\sqrt{(s-1)gd^*}d^*}{\nu}, \tag{2.3}$$

where s is the relative density of the sediment, g is the gravitational acceleration and d^* is the median diameter of the sediment mixture used in the experiments. The roughness Reynolds number Re_k may be related to the above parameters as follows:

$$Re_k = \sqrt{\theta} Re_p \frac{k_s^*}{d^*}, \tag{2.4}$$

where k_s^* has been set equal to $2.5d^*$.

In figure 1(a) the experiments of Guy *et al.* (1966) that are relevant for the present analysis are presented in the classical Shields diagram. The experimental data span about a decade in the particle Reynolds number and in the Shields parameter. The dotted lines represent curves at values of Re_k equal to 5 and 70, thus bounding the transitional regime from the smooth and the rough regimes, respectively. The solid line represents the critical value of the Shields parameter θ_c for incipient motion of the sediment, here expressed in terms of Re_p through the relationship (Brownlie 1981)

$$\theta_c = 0.22 Re_p^{-0.6} + 0.06 \exp\left(-17.73 Re_p^{-0.6}\right). \tag{2.5}$$

Moreover, hollow markers denote 'transitional' bed configurations, i.e. runs in which the experimenters detected the simultaneous presence of both ripples and dunes or of isolated ripples over an otherwise plane bed. This specification allows for the identification of the ripple existence region as

$$\theta_c < \theta < 3.5\theta_c \cup Re_k < 25, \tag{2.6}$$

https://doi.org/10.1017/S0022112011000048 Published online by Cambridge University Press

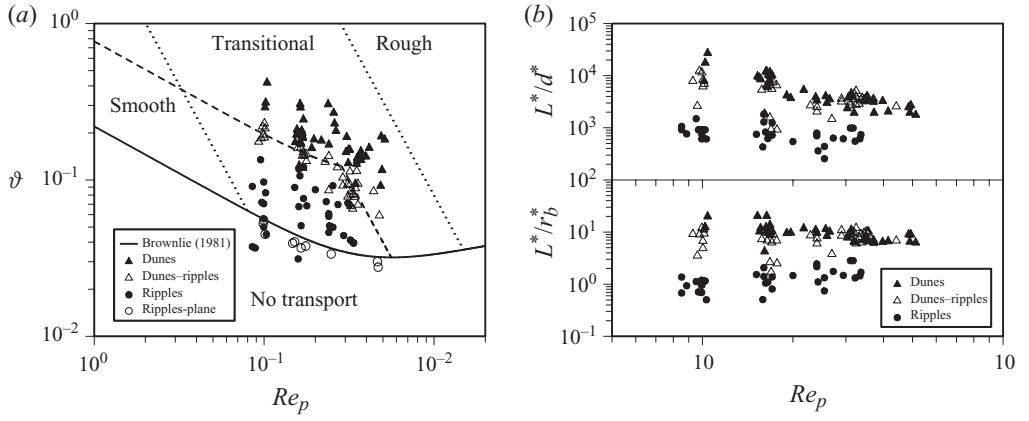


FIGURE 1. Ripples and dunes experiments of Guy *et al.* (1966) in a Shields diagram (*a*) and (*b*) corresponding wavelengths scaled with the sediment diameter d^* (upper panel) and with the bed hydraulic radius r_b^* (lower panel).

the border of which is represented as a dashed line in the plot.

It is worth noting that 'dune–ripple' data have been classified as 'dune' by Guy *et al.* (1966), who accordingly provided just one measured wavelength, the presence of ripples being only acknowledged in the detailed notes accompanying each experiment. Moreover, the coarsest data set ($d^* = 0.93$ mm) of the experiments of Guy *et al.* (1966) has been excluded from the analysis, since no ripples have been observed in this set of experiments regardless of the value of the Shields parameter.

The experimental values of dune and ripple wavelengths are presented in figure 1(*b*), scaled with the sediment diameter d^* and with the bed hydraulic radius r_b^*, in the upper and lower panels, respectively. For the experimental range of Re_p considered, ripple wavelengths seem better correlated with the sediment diameter, since their ratio is found to attain an almost constant value of about 1000, as predicted by Yalin (1977), although a fairly large scatter is present. The opposite is true for dune wavelengths, which better scale with the bed hydraulic radius with a value of the ratio of about 10. It must be pointed out that, irrespective of the scaling adopted, in both panels the characteristic wavelengths for dunes and ripples are separated by about one decade. Since our purpose was to investigate the transition from ripples to dunes, our choice for the scaling fell naturally on the bed hydraulic radius r_b^*.

3. Formulation of the problem

The formulation follows closely the one adopted by Colombini (2004) and by Colombini & Stocchino (2005, 2008), which is briefly summarized in the following. The interested reader is referred to the above works for the details of the flow and the sediment transport models.

A uniform turbulent free-surface flow in an infinitely wide straight channel is considered. The triplet composed of the fluid density ρ, the mean friction velocity u_f^* and the depth D^* of the unperturbed uniform flow has been used for non-dimensionalization. Note that by formally setting D^* equal to r_b^*, u_f^* devolves to u_b^* and all the relationships introduced in the previous section remain valid in the infinitely wide configuration adopted herein. In particular, the wavelength-to-depth ratio is adopted in the following to set ripples apart from dunes.

https://doi.org/10.1017/S0022112011000048 Published online by Cambridge University Press

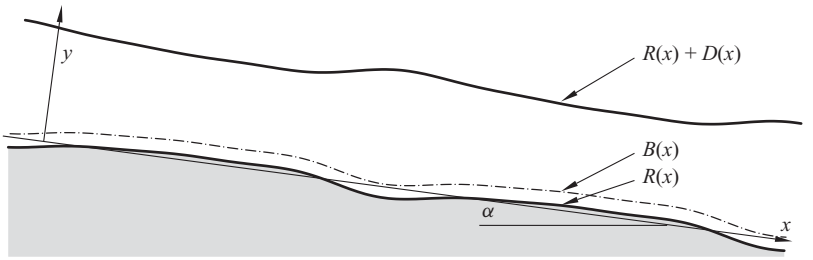


FIGURE 2. Sketch of flow configuration.

In the sloping Cartesian coordinate system (x, y), sketched in figure 2, the dimensionless unsteady Reynolds and continuity equations read

$$U_{,t} + UU_{,x} + VU_{,y} + P_{,x} - SC^2/F^2 - T_{xx,x} - T_{xy,y} = 0, \tag{3.1}$$

$$V_{,t} + UV_{,x} + VV_{,y} + P_{,y} + C^2/F^2 - T_{xy,x} - T_{yy,y} = 0, \tag{3.2}$$

$$U_{,x} + V_{,y} = 0, \tag{3.3}$$

where $\boldsymbol{U} = (U, V)$ is the velocity vector averaged over turbulence, P is the pressure, $\boldsymbol{T} = \{T_{ij}\}$ is the total (viscous plus Reynolds) two-dimensional stress tensor, $F = U^*/\sqrt{gD^*}$ is the Froude number and S is the mean bed slope.

The above system is complemented by the Exner equation imposing mass conservation of sediments, which takes the dimensionless form:

$$R_{,t} - Q\Phi_{,x} = 0, \quad Q = \frac{d\sqrt{\theta_0}}{(1-p_s)}, \quad \theta_0 = \frac{F^2}{C^2(s-1)d}, \tag{3.4}$$

where R is the bed elevation, Φ is the sediment transport capacity per unit width, d is the sediment grain size, assumed as uniform, p_s is the sediment porosity and θ_0 is the Shields parameter for the base uniform flow. It may be worth noting that the latter is proportional to the square of the Froude number F.

The following transformation of variables:

$$\eta = \frac{y - R(\xi, \tau)}{D(\xi, \tau)}, \quad \xi = x, \quad \tau = t, \tag{3.5}$$

is then employed to map the domain shown in figure 2 into a rectangular domain.

In order to extend the flow model to cover the smooth and transitional regimes, a modified mixing length structure along the vertical is adopted:

$$l = \kappa(\eta + \Delta\eta)D\left[1 - \exp\left(-\frac{\eta + \Delta\eta}{A}D\frac{Re_k}{k_s}\right)\right](1-\eta)^{\frac{1}{2}}, \tag{3.6}$$

where D and k_s are the dimensionless local flow depth and bed roughness, respectively. The exponential correction appearing in (3.6) accounts for the existence of a viscous and buffer layer in the hydraulically smooth regime, the damping factor A taking a value of 27 (van Driest 1956). Moreover, a shift $\Delta\eta$ is introduced as suggested by Rotta (1962), who recognized that the velocity profiles for smooth and rough wall can be similar provided that the vertical coordinate is suitably displaced.

The displacement $\Delta\eta$ has been computed, as in Sumer & Bakioglu (1984), in terms of Re_k by means of the relation, in wall coordinates, suggested by Cebeci & Chang

https://doi.org/10.1017/S0022112011000048 Published online by Cambridge University Press

(1978):

$$\Delta\eta^+ = 0.9\left[\sqrt{Re_k} - Re_k \exp\left(-\frac{Re_k}{6}\right)\right]. \tag{3.7}$$

Note that, by means of numerical integration of the velocity vertical profile for a uniform flow, a link can be established between the displacement $\Delta\eta$ and the conductance coefficient C given by (2.1)–(2.2), as is usually done in fully rough flows, where $\Delta\eta$ should become formally equivalent to the roughness height z_0 (Rotta 1962). In other words, in the smooth and transitional regimes, (3.7) can be obtained from (2.1) and (2.2) and vice versa.

Finally, a dependence of the critical Shields stress on Re_p through (2.5) has been included in the analysis. This enters directly in the evaluations of the sediment transport capacity Φ and of the level η_b at which the shear stress must be evaluated, the latter being a crucial quantity in the estimate of the phase lag between the bed shear stress and the bed elevation that, ultimately, drives the process of instability. We recall here that η_b is related to the ratio θ_0/θ_c by means of an empirical relationship which allows for the determination of the average saltation height of the sediments and, in turn, of the bedload layer thickness. The inclusion of the θ_c dependence on Re_p is certainly the simplest way to introduce a viscous scale in the sediment transport model. Unfortunately, the lack of experimental observations on the behaviour of the saltation height in the smooth and transitional regimes did not allow for a more accurate modelling of sediment dynamics.

4. Linear analysis

The problem is solved in terms of normal modes, expanding a generic quantity G as

$$G(\xi, \eta, \tau) = G_0(\eta) + \epsilon G_1(\eta)\exp[\mathrm{i}k(\xi - \omega\tau)]\exp(\Omega\tau) + \text{c.c.}, \tag{4.1}$$

where ϵ is a small parameter and k, ω and Ω are wavenumber, celerity and growth rate of the perturbation, respectively.

Substituting the above expansion into the governing equations, boundary conditions and turbulence closure and collecting terms of the same order of magnitude in ϵ, a sequence of differential problems arises.

At leading order, a velocity vertical profile is obtained that, as expected, asymptotically devolves to the classical logarithmic distributions valid for the hydraulically smooth and rough regimes.

At the linear level, an eigenvalue problem is recovered, which yields a dispersion relation of the kind

$$\Omega = QBk^2\left(\frac{T_{t1b}}{k} - \frac{\mu}{\theta_0}\right), \tag{4.2}$$

where T_{t1b} is the imaginary part of the perturbation of the shear stress evaluated at the level η_b, μ is the gravity correction coefficient taken as 0.1 (Fredsøe 1974) and B is a parameter that depends solely on the sediment transport parameters of the base uniform flow. In particular, (4.2) shows that instability is recovered when the perturbed bed shear stress leads the bed perturbation ($T_{t1b} > 0$). The stabilizing role of gravity is also shown to decrease as θ_0 increases.

Once again, this result is formally equivalent to the one reported by Colombini & Stocchino (2008). The novelty of the present formulation is contained in the perturbation of the bed shear stress, which now displays a dependence on the

https://doi.org/10.1017/S0022112011000048 Published online by Cambridge University Press

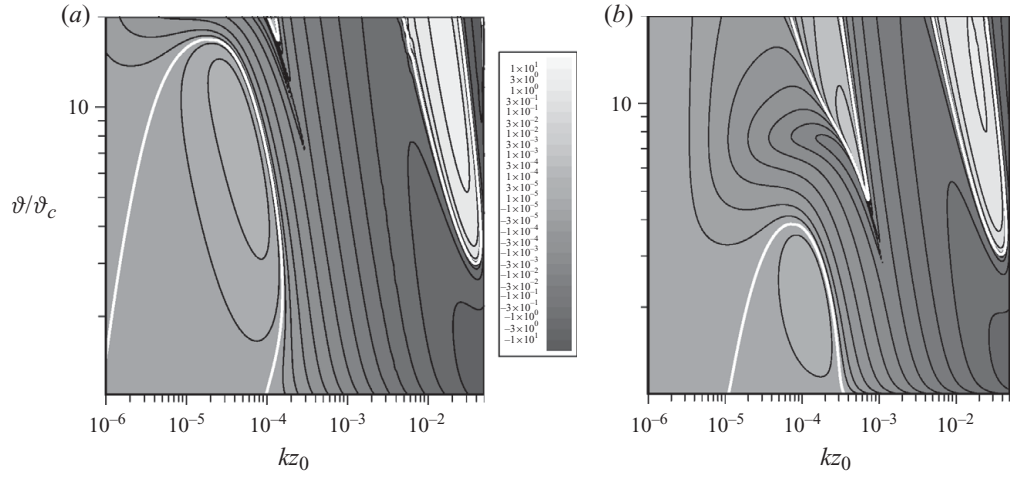


FIGURE 3. Stability plot in the rough regime, $Re_p = 700$: (*a*) $z_0 = 10^{-4}$; (*b*) $z_0 = 5 \times 10^{-4}$. Solid white lines indicate marginal curves.

roughness Reynolds number Re_k, thus extending the previous analysis to cover the case of smooth and transitional regimes, as required to investigate ripple formation. To simplify the analysis we have restricted our attention to the decoupled case, thus disregarding time derivatives in the flow equations, so that only one eigenvalue is obtained from (4.2).

5. Discussion of results

We start our discussion by focusing on the rough regime, where the present analysis recovers the results of Richards (1980). Our purpose is to show how the instability associated with ripples in the latter work was indeed generated by the inability of the flow model to predict the correct bed shear stress for values of the wavenumber that are of the order of the roughness height. To do so, we simply set the displacement $\Delta\eta$ to be equal to the roughness height z_0 (Rotta 1962):

$$\Delta\eta = z_0 \simeq \frac{k_s}{30} = \frac{d}{12}. \tag{5.1}$$

Stability plots in the $(kz_0, \theta_0/\theta_c)$ plane are shown in figure 3 as contours of the growth rate Ω for values of z_0 equal to 10^{-4} and 5×10^{-4}, respectively. The growth rate is shown in shades of grey, lighter colours corresponding to higher values in a logarithmic scale. Marginal curves are shown as solid white lines.

The stability diagram shown in figure 3(*a*) has been obtained with the same value of z_0 of Richards (1980) to allow for a direct comparison with the results presented in figure 5 of his work. The largest region of instability for values of kz_0 of order $O(10^{-5})$ can be easily associated with dune instability, whereas ripples were postulated by Richards (1980) to be represented by the second region of instability, characterized by larger $O(10^{-2})$ wavenumbers. Increasing z_0, i.e. considering coarser sediment, as in figure 3(*b*), the region of instability for dunes contracts, the anti-dune mode appears for higher values of θ_0, whereas the instability region at higher wavenumbers remains almost unchanged. These results clearly show that the latter mode of instability cannot be associated either with ripples or with any actual physical instability of the bed.

https://doi.org/10.1017/S0022112011000048 Published online by Cambridge University Press

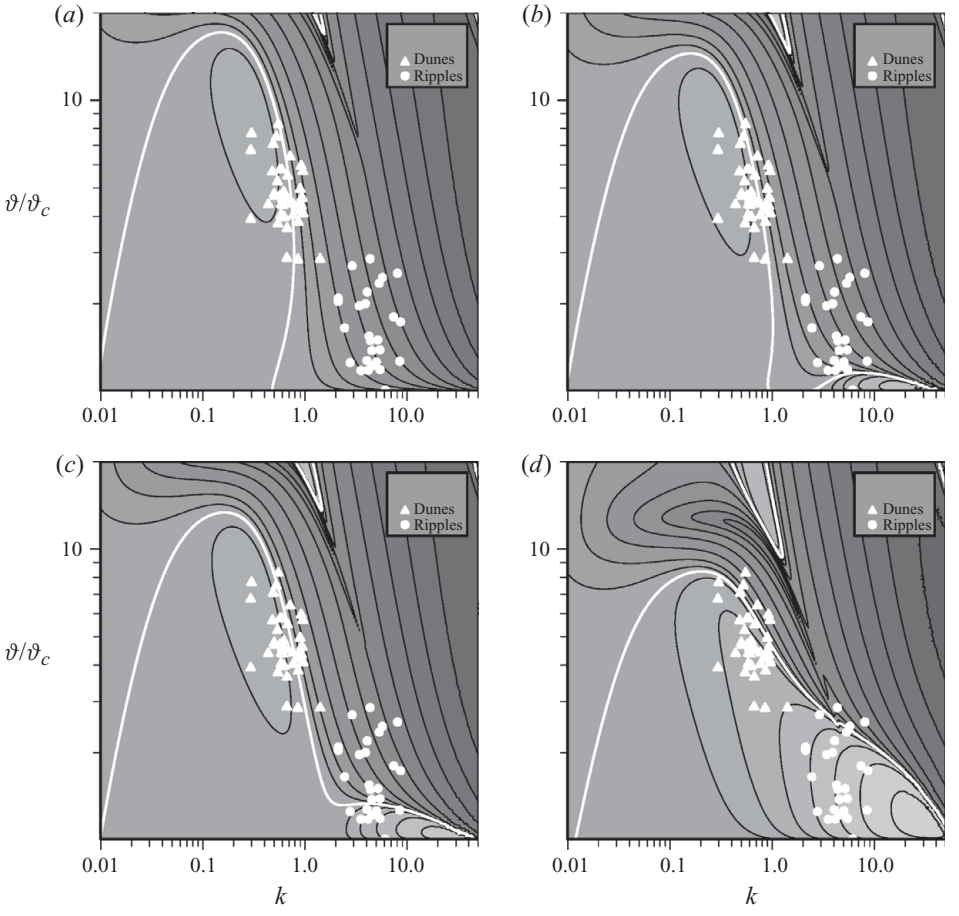


FIGURE 4. Stability plots in the hydraulically smooth and transitional regimes: (*a*) $Re_p = 20$; (*b*) $Re_p = 14$; (*c*) $Re_p = 12$; (*d*) $Re_p = 5$. Markers denote the experimental runs of Guy *et al.* (1966) (see figure 1). The colourmap is the same as in figure 3.

Note that the values of kz_0 of $O(10^{-2})$ correspond to wavenumbers scaled with the bed roughness of $O(1)$, z_0 being about 1/30th of k_s. Therefore, the appearance of this spurious mode of instability simply reveals that the flow model is incapable of resolving scales of the order of the bed roughness. This can be considered as an intrinsic limit of the representation of rough turbulent flows by Reynolds-averaged models, such as Richard's and the present one, as well as by more sophisticated flow models (Fourrière *et al.* 2010).

We now proceed to analyse the case of smooth and transitional flow regimes, with the purpose of showing how ripple instability can indeed be described by the present model, hence providing a unified linear framework for both ripple and dune formation.

In figure 4 the stability plots for several values of Re_p are presented as a function of the wavenumber k, built upon the wavelength-to-depth ratio, together with the experimental observations of Guy *et al.* (1966) pertaining to either dunes or ripples (i.e. disregarding the mixed dune–ripple data, for which only one measured wavelength was available). For the highest value of Re_p (*a*), only one region of instability is

https://doi.org/10.1017/S0022112011000048 Published online by Cambridge University Press

found, which can be associated with dunes ($k = O(1)$). Decreasing Re_p down to 14 (b), a second region of instability appears in the large wavenumber range ($k = O(10)$), which can be related to ripples. As the particle Reynolds number is further decreased (c) the two regions merge. Two separate maxima in the growth rate persist down to a value of Re_p of about 10, below which a single maximum exists (d). Therefore, the present theory predicts that, for intermediate Re_p, two distinct wavenumbers of maximum amplification exist, which can be associated with ripples and dunes, respectively. Although no information can be gathered at a linear level on which mode of instability, if one, would eventually prevail on the other, we regard this result as an important confirmation of our analysis, since the experimental observations of Guy *et al.* (1966) enlighten that ripples and dunes may coexist. Finally, note that, for very small grain sizes, the wavenumber of maximum amplification varies continuously from values typical of ripples to the ones of dunes as θ_0 is increased.

The stability diagrams shown in figure 4 have been obtained for a value of k_s equal to 0.003, which corresponds to a value of $z_0 = 10^{-4}$, representative of most of the experimental runs regarding both ripples and dunes. Note that, by this choice, the maximum value of k in the plots corresponds to a wavenumber scaled with the bed roughness of $O(10^{-1})$, hence on the safe side regarding the above discussion for the rough regime. Nonetheless, the spurious instability persists also in the smooth and transitional regimes, thus confirming that it is related to an intrinsic limitation of the flow model. In each plot, as Re_k increases along the vertical axis following (2.4), the flow shifts from the smooth towards the transitional and rough regimes. The choice of keeping Re_p constant, instead of the more obvious one of fixing Re_k, has been made in order to make each plot representative of an ideal experiment in which the dimensional grain size is fixed and so does the dimensional flow depth of the base flow (since k_s is fixed), whereas θ_0, F and Re_k vary as the dimensional average flow velocity is increased.

It must be pointed out that the present results display a fairly good agreement between observed and predicted (in terms of maximum amplification) ripple wavenumbers, whereas the analyses of both Richards (1980) and Sumer & Bakioglu (1984) failed to do so, their predictions on wavelengths being about one order of magnitude too short. However, the upper limit of Re_p for ripple instability predicted by the present analysis is about 15, a value that underestimates the observed one by a factor of about 2 (see figure 1a), whereas, in this regard, the work of Sumer & Bakioglu (1984) provided an excellent agreement with observations. A possible explanation for this discrepancy might be sought in the scarcity of information available on the sediment transport (and in particular on the saltation height) in the smooth and transitional regimes.

6. Conclusions

A linear stability analysis of dune and ripple formation has been presented, which extends previous works on the subject to cover the case of smooth and transitional flows. Results are shown to depend on two parameters that characterize the flow and the sediment, namely the Shields parameter and the particle Reynolds number or, equivalently, on the Froude number and the roughness Reynolds number. Both these parameters are then relevant for the process of instability and this might explain why previous theories, being developed in the limit of either vanishing Froude number or large roughness Reynolds number, failed to predict the occurrence of both ripples and dunes in the same framework of instability.

https://doi.org/10.1017/S0022112011000048 Published online by Cambridge University Press

By an analysis of the fully rough case, it is shown that care must be taken when investigating the range of wavelengths of the order of bed roughness, where the flow model fails. This led Richards (1980) to erroneously associate this spurious instability with ripple formation.

Results obtained in the smooth and transitional regimes clearly indicate that both ripples and dunes appear as a primary instability. This is in contrast with the arguments sustained by Fourrière *et al.* (2010), who considered ripples as the only form of primary instability, whereas dunes were obtained through a mechanism of nonlinear pattern coarsening. In this regard, we also recall that modal analyses like the present one are known to provide only the asymptotic response of the system in time, whereas during the transient (from plane bed to small amplitude bedforms still in the linear regime) shorter disturbances can develop that experience an increase in wavelength (Camporeale & Ridolfi 2009).

The present results confirm the validity of the approach of Sumer & Bakioglu (1984), whose analysis has been extended here to cover the effect of flow depth. It is found that, although ripple formation is also controlled by the viscous scale, the latter cannot be used alone in the determination of the characteristic wavelengths, since, similarly to the case of dunes, flow depth plays a role as well.

As a final comment, we would like to recall the definition of dunes given by Guy *et al.* (1996) and cited in § 1: dunes form at larger values of θ, whereas ripples form at smaller values of θ. At intermediate values of θ, they may coexist. With a suitable choice of Re_p, the present analysis qualitatively reproduces all the above behaviours: at lower values of θ ripples tend to dominate dunes, whereas the opposite is true for higher values of θ. Dunes and ripples may also coexist (two maxima) for intermediate values of θ. The quantitative agreement of the present results with observations in terms of characteristic wavelengths is fairly good, whereas in terms of both θ and Re_p is not equally satisfactory.

REFERENCES

ASCE Task Committee 1963 Friction factors in open channels. *J. Hydraul. Div.* **89**, 97–143 (HY2).

Brownlie, W. R. 1981 Prediction of flow depth and sediment discharge in open channels. *Tech. Rep.* KH-R-43A. California Institute of Technology, Pasadena, California.

Camporeale, C. & Ridolfi, L. 2009 Nonnormality and transient behavior of the de Saint-Venant–Exner equations. *Water Resour. Res.* **45**, W08418.

Cebeci, T. & Chang, K. C. 1978 Calculation of incompressible rough-wall boundary-layer flows. *AIAA J.* **16**, 730–735.

Cheng, N.-S. 2008 Formulas for friction factor in transitional regimes. *J. Hydraul. Engng* **134**, 1357–1362.

Coleman, S. E. & Melville, B. W. 1996 Initiation of bed forms on a flat sand bed. *J. Hydraul. Engng* **122**, 301–310.

Colombini, M. 2004 Revisiting the linear theory of sand dune formation. *J. Fluid Mech.* **502**, 1–16.

Colombini, M. & Stocchino, A. 2005 Coupling or decoupling bed and flow dynamics: fast and slow sediment waves at high Froude numbers. *Phys. Fluids* **17** (3), 9.

Colombini, M. & Stocchino, A. 2008 Finite-amplitude river dunes. *J. Fluid Mech.* **611**, 283–306.

van Driest, E. R. 1956 On turbulent flow near a wall. *J. Aeronaut. Sci.* **23**, 1007–1011, 1036.

Engelund, F. & Fredsøe, J. 1982 Sediment ripples and dunes. *Annu. Rev. Fluid Mech.* **14**, 13–37.

Fourrière, A., Claudin, P. & Andreotti, B. 2010 Bedforms in a turbulent stream: formation of ripples by primary linear instability and of dunes by nonlinear pattern coarsening. *J. Fluid Mech.* **649**, 287–328.

Fredsøe, J. 1974 On the development of dunes in erodible channels. *J. Fluid Mech.* **64**, 1–16.

https://doi.org/10.1017/S0022112011000048 Published online by Cambridge University Press

Guy, H. P., Simons, D. B. & Richardson, E. V. 1966 Summary of alluvial channel data from flume experiments 1956-61. *Prof. Paper* 462-I. U.S. Geol. Survey.

Kobayashi, N. & Madsen, O. S. 1985 Formation of ripples in erodible channels. *J. Geophys. Res.* **90**, 7332–7340.

Raudkivi, A. J. 2007 Transition from ripples to dunes. *J. Hydraul. Engng* **132**, 1316–1320.

Richards, K. J. 1980 The formation of ripples and dunes on an erodible bed. *J. Fluid Mech.* **99**, 597–618.

Rotta, J. C. 1962 Turbulent boundary layers in incompressible flow. *Prog. Aerosp. Sci.* **2**, 1–219.

Sumer, B. M. & Bakioglu, M. 1984 On the formation of ripples on an erodible bed. *J. Fluid Mech.* **144**, 177–190.

Yalin, M. S. 1977 On the determination of ripple length. *J. Hydraul. Div. ASCE* **103**, 439–442.

https://doi.org/10.1017/S0022112011000048 Published online by Cambridge University Press